# Dynamics of mutual inhibition between two visual cortical neurons compared to human perceptual competition

Naoki Kogo[1]

Felix B. Kern[2]

Thomas Nowotny[3]

Raymond van Ee[4,5]

Richard van Wezel[1,6]

Takeshi Aihara[7]

Paste the full affiliation list here.

[1]Biophysics, Donders Institute for Brain, Cognition and Behaviour, Radboud University, The Netherlands

[2]School of Life Sciences, Sussex Neuroscience, University of Sussex, UK

[3]School of Engineering and Informatics, University of Sussex, UK

[4]Biophysics, Donders Institute for Brain, Cognition and Behaviour, Radboud University, The Netherlands

[5]Brain and Cognition, University of Leuven, Belgium

[6]Biomedical Signals and Systems, MedTech Centre, University of Twente, The Netherlands

[7]Graduate School of Brain Sciences, Tamagawa University, Japan

**Abstract**

Visual perception emerges as the result of neural systems actively organizing intrinsically noisy visual signals. It is commonly assumed that selection processes of competing neurons underlie this emergence of perceptual organization. While the neural competition, realized by such a “mutual inhibition” circuit has been examined in many theoretical studies, its dynamic properties have not been investigated in real neurons. We have developed a “hybrid” system where two real-life pyramidal neurons in a mouse brain slice interact through a computer simulated mutual inhibition circuit. We found that simultaneous activation of the mutually inhibiting pyramidal neurons leads to bi-stable activity. We investigated the effects of noise and the effect of changes in the activation strength on the dynamics. We observed that the circuit exhibits dynamics strikingly similar to the known properties of bi-stable visual perception.

## Main Text

### Introduction

"Bi-stable perception" occurs when visual signals support two likely perceptual interpretations[1]. Neural competition is assumed to underlie the bi-stability and is modelled by "mutual inhibition" between competing neurons. In a mutual inhibition circuit, each pyramidal neuron (PN1 and PN2 in Figure 1a) activates a partner inhibitory neuron (IN1 and IN2) which, in turn, projects an inhibitory synapse to the competing pyramidal neuron. It has been suggested that the conflicting signals for local features such as orientation[2,3], motion direction[4,5], and edge assignment[6,7] compete through such mutual inhibition circuits. The concept of mutual inhibition is also found in many models for other signal processing such as object recognition[8], decision-making[9,10], and place cell field [11]. It is hence possible that mutual inhibition works as a canonical building block. However, thorough neurophysiological studies of mutual inhibition in cortical neurons are missing. Therefore, the details of interplays between neural adaptation, noise and stimulus intensity in real-life neural system are unknown.

We established an experimental model where a model mutual inhibition circuit is constructed between a pair of real-life pyramidal neurons (Figure 1b). This hybrid system has the advantage of keeping physiological properties of the real pyramidal neurons intact, while providing full control over the simulated connections between them. Using this system, we succeeded to evoke bi-stable activity in the pyramidal neurons in visual cortex. We investigated the dynamics of the bi-stable activity and compared them with the known dynamics of bi-stable visual perception.

### Results

Double patch clamp recordings were performed from pyramidal neurons in layer 2/3 of mouse primary visual cortex in brain slice preparation (Figure 1c, 93 pairs from 32 mice). Some pyramidal

neuron pairs were biocytin-filled and visualized after the experiments (N=9) and the stereotypical morphology of pyramidal neurons was identified, located in layer 2/3 of V1 (Figure 1d).

Mutual inhibitory connections between each pair of pyramidal neurons were constructed by a dynamic clamp system (spike timing dependent plasticity clamp, StdpC[12,13]). The inhibitory neurons were modeled (mINs) by implementing Hodgkin-Huxley type ion channel models. The connections between the (real) pyramidal neurons and the (model) inhibitory neurons were established with modelled excitatory and inhibitory synapses. In Figure 2a, an action potential of pyramidal neuron 1 (PN1) was evoked by the injection of a brief depolarization current (red triangle). This action potential activated the model inhibitory neuron, and, in turn, triggered an inhibitory synaptic current injected into pyramidal neuron 2 (PN2) (supplement Figure S1). This evoked an inhibitory postsynaptic potential (IPSP) in PN2 (blue asterisk in Figure 2a). When an action potential was evoked in PN2 (blue triangle), a modelled IPSP was evoked in PN1 (red asterisk), illustrating that a mutual inhibition was established.

**Bi-stable activity**

When continuous depolarization currents were injected into PN1 and PN2 simultaneously, bi-stable activity with alternating dominance between the two pyramidal neurons was evoked (Figure 2b). In this example, both neurons started to depolarize but PN2 reached the action potential threshold before PN1 and, hence, PN1 received the evoked IPSP before succeeding to generate an action potential (Figure 2c). Thereafter, PN2 showed sustained firing of action potentials and it achieved initial dominance. Note an increase of inter-spike intervals in PN2 and a ramp-like slow depolarization in PN1 (Figure 2b). The former is a sign of adaptation while the latter indicates the decreasing effect of inhibition from the other neuron. While the inter-spike interval in PN2 increased, PN1 recovered more from IPSPs. The inter-spike interval of PN2 eventually became long enough such that the membrane potential of PN1 reached the action potential threshold before PN2 could

generate another action potential. Consequently, PN2 received an IPSP evoked by the first action potential of PN1 (Figure 2d). From then on, PN1 became dominant and PN2 became suppressed.

Inter-spike intervals and peaks of action potentials are plotted (Figure 3a, b, for the example in Figure 2b, and Figure 3c, d for the "control pairs" (N=93), see Methods for the definition). Inter-spike intervals increase and action potential peaks decrease monotonically over time. The dominance durations and the changes of the inter-spike intervals correlated. A linear regression to inter-spike intervals was applied as a function of time in the dominance duration (supplemental Figure S3). The slopes and the dominance durations were inversely correlated (Figure 3e for the example in Figure 2b, and Figure 3f for the control pairs, repeated measures ANOVA $F(3,15)=19.518, p<0.0001$), indicating a role for adaptation in dominance reversals.

**Effect of noise**

It has been argued that noise plays an important role in bi-stable perception[14–17]. We implemented an algorithm in the dynamic clamp to introduce simulated synaptic noise[18,19]. The noise was given to both PNs and mINs in the form of random fluctuations of excitatory and inhibitory synaptic conductance. Figure 4a shows the baseline membrane potential of a pyramidal neuron and Figure 4b shows the result of adding the modeled synaptic noise to it. Next, the level of noise was changed systematically while the two pyramidal neurons exhibited bi-stable activity (Figure 4c, see the table in Figure 4d for the parameter sets for different noise level). The increase of noise caused an increase of the reversal rate ($F(19,171)=50.868, p<0.0001$). The pooled data from 15 pairs of pyramidal neurons are shown in Figure 4d.

In brain slice preparations, synaptic noise is less than for intact brain preparations due to the cutoff of axons and lesser spontaneous activity[18]. Therefore, to reproduce the intact brain environment, we used a parameter set of modelled synaptic noise which will be called the "standard noise parameter set" (asterisk in Figure 4c, 4d and Table 1). For the rest of the experiments, the standard set was used. The histogram of dominance durations of a 600 sec recording shows a skewed

distribution as stereotypically observed in bi-stable perception (Figure 4e). The average of dominance durations and reversal rates of the 15 pairs with the standard noise parameter set were 7.7±5.6sec and 12.0±10.5min$^{-1}$, respectively. These values for the control pairs (N=93) were 8.2±7.8sec and 11.5±10.8min$^{-1}$, respectively.

**Effect of current intensity**

Laws of perceptual competition —known as Levelt's propositions— describe the relationship between the strengths of two competing stimuli and the dynamics of their bi-stable perception[20]. To examine whether the pairs of mutually inhibiting pyramidal neurons also exhibit dynamics that are in line with Levelt's propositions, we systematically varied the strength of the current into one, or both, of the pyramidal neurons (Figure 5a).

To examine the first three propositions of Levelt, the current injected into one of the two neurons was varied while the current injected into the other neuron was kept constant (Fig 5b). In total, 46 pairs were recorded with this paradigm. To pool the data, first, the current that would evoke 50% dominance (the total period that one neuron is dominant is equal for both neurons) was estimated ($I_{50\%}$) by linear regression of dominance over the changed current. The change of the current is reported with reference to this control value. Hence, in Figure 5c to 5h, the neurons with the changed current (red) are "stronger" than the neuron without change of current (blue) on the right side of the plot from 0, and "weaker" on the left side.

We first tested Levelt's proposition I: Increasing stimulus strength for one of the competing stimuli will increase the perceptual dominance of that stimulus. Figure 5c depicts the change of the dominance ratios of the two pyramidal neurons over injected current for the example shown in Figure 5b. There is an increase of dominance of PN1 whose current was increased and a decrease of dominance of PN2 whose current was kept constant. Figure 5f shows pooled data (N=46) replicating the increasing dominance of the neurons whose currents were increased (red,

*F(6,24)=15.558, p<0.0001*), and the decreasing dominance for their counterparts (blue, *F(6,24)=15.558, p<0.0001*)). This is in line with Levelt's proposition I.

Proposition II states: Increasing the difference in stimulus strength between the two competing stimuli will primarily act to increase the average perceptual dominance duration of the stronger stimulus. In Figure 5d the change of the average dominance durations is plotted over the changing current for the example shown in Figure 5b. PN1 shows weak changes of the dominance durations on the left half of the plot where PN1 is weaker than PN2 and a steep increase on the right half of the plot where it is stronger than PN2 (vice versa for the other neuron). Hence, the dominant neuron shows a steep increase of the dominance durations with current values deviating further away from $I_{50\%}$. This trend can be seen in Figure 5g with pooled data for the neurons whose currents were increased (red, *F(6,24)=4.371, p<0.01*)) and for their counter parts (blue, *F(6,24)=7.396, p<0.0001*). This is in line with Levelt's proposition II.

Proposition III states: Increasing the difference in stimulus strength between the two competing stimuli will reduce the perceptual alternation rate. Figure 5e plots the number of reversals for the example shown in Figure 5b. The pair showed a higher number of reversals for a current close to $I_{50\%}$. Deviating further from $I_{50\%}$ in either direction, the values decreased, in line with Levelt's proposition III. However, the pooled data (Figure 5h) show that the response is not symmetric. In fact, some pairs showed an increase of the reversal rate when a neuron is dominant in contrast to the example pair of Fig 5b (see Supplement Figure S4). Thus, the pyramidal neuron pairs did not always follow Levelt's proposition III. Due to the increase in the left half, repeated measures ANOVA indicated a significant effect (*F(6,24)=2.663, p<0.05*).

Proposition IV states: Increasing stimulus strength of both competing stimuli will generally increase the perceptual alternation rate. To examine this proposition, the currents injected into both neurons were varied. 32 pairs were recorded with this paradigm. To pool the data, the change of the current is reported with reference to the current that would evoke approximately 10Hz ($I_{10Hz}$, see Methods). Figure 6a shows an example of the effect of increasing the injected currents into both neurons. In

Figure 6b, the number of reversals of this example are plotted over the injected current. Figure 6c shows pooled data indicating increasing reversal rates ($F(6,30)=4.051, p<0.01$). This is in line with Levelt's proposition IV.

## Discussion

Using a system to establish a mutual inhibition connection between two real-life neurons mediated by model neurons and synapses, bi-stable activity was evoked in a pair of pyramidal neurons in visual cortex. We analyzed the dynamics of the bi-stability and the effects of the level of background noise and activation level. We compared the dynamics of this experimental model with the known dynamics of human bi-stable visual perception. Although our experimental system represents the simplest neural unit of competition and human behavior represents the most complex system, we found that the two systems show striking similarities in their dynamics.

The analyses of the physiological properties during bi-stable activity showed neural adaptation of the dominant neurons (Figure 3a to d). Up until now, neural adaptation has only been *assumed* as a key element for bi-stability theoretically [17,21–24], and *supported indirectly* in the form of decreased contrast sensitivity[25]. Our data are the first to directly show, in physiological terms, a progression of adaptation during bi-stable activity in pyramidal neurons in visual cortex and a causal link between neural adaptation and the reversals (Figure 3e and f) in bi-stable activity.

We also investigated the effect of neural noise on the dynamics of bi-stable activity. The apparent stochasticity in the sequence of reversals and the skewed distribution of dominance durations in bi-stable perception[26] led to studies on the role of noise[14–17]. We incorporated a computational model of synaptic noise into the dynamic clamp system to insert noise into the pyramidal and inhibitory neurons and systematically changed the level of noise. We found that an increase of noise caused an increase of reversal rate and that the histogram of dominance durations was right-skewed as is typically found in bi-stable perception.

We showed that adaptation of the dominant neuron progresses and hence the inter-spike interval increases over time. This allows the suppressed neuron to depolarize more during the ever-increasing inter-spike intervals of the dominant neuron, consequently showing a slowly ramping depolarization. When the depolarized membrane potential comes close to the firing threshold, the noise facilitates the membrane potential to go above the threshold. Finally, the suppressed neuron evokes action potentials and the dominant neuron now receives IPSPs and a reversal occurs. Hence, our data elucidate the dynamic interplay between adaptation, noise and mutual inhibition in determining the dynamics of bi-stable activity.

Our experimental model allowed us to separately manipulate the levels of activation of the competing neurons. Hence, it enabled us to compare the effects of changing activation levels in pyramidal neurons to the dynamics of bi-stable activity with the effects of changes in stimulus strength on the dynamics of bi-stable perception, as described in Levelt's four propositions[20]. Propositions I, II and III make predictions about the changes of dominance, the dominance durations, and the reversal rate, respectively, in response to changes of the stimulation strength in one of the two inputs. Proposition IV concerns the change in the reversal rate while the stimulus strengths of both inputs are changed concurrently. The original propositions were modified later[14,27] to cover the whole range of the stimulus strength. By running paradigms equivalent to these experiments, we found that both systems show striking similarities in their dynamics.

One exception, however, was the mixed results for the Levelt III paradigm. In this paradigm, some pyramidal neuron pairs showed a decrease of reversal rates when the depolarization current either increased or decreased from the control value, $I_{50\%}$, which is in line with Levelt's proposition III. However, other pairs showed an increase of reversal rate when the current was higher than the control. Note that the reversal rate is determined by the balance between increased dominance durations of the stronger neuron and decreased dominance durations of the weaker neuron. If the former is more significant, the reversal rate will decrease and if the latter is more significant, it will increase. The mixed results suggest that multiple factors determine the final outcome in the reversal

rate. The increase of the firing rate in the stronger neuron may cause a stronger dominance of the neuron on one hand, and a stronger adaptation of the neuron on the other hand. The latter may prevent the increase of the dominant durations due to the faster decay of the firing rate. Hence, depending on the individually different adaptation properties and the spiking properties of the neurons, the strong activation of the stronger neuron may have caused a decrease of the reversal rate in some cases and an increase in other cases. At systems level, the competition is between populations of neurons rather than single neurons as tested here. Hence, differences in adaptation and spiking properties among the involved neurons may collectively have different impacts on the dynamics of bi-stability. Furthermore, in the human brain, the input signals go through multiple steps of normalization, starting from the retinae, before reaching the mutual inhibition processes. It may be possible that the activation level of neurons in the human visual system is kept within the range where the fast adaptation occurs in a lesser amount. If this is the case, the strong stimulation would cause the prolongation of dominant durations in the stronger neuron and, hence, cause the decrease of the reversal rate as reported in Levelt III.

Two intriguing phenomena regarding the dominance durations were observed. First, there are short periods when the neuron that has been suppressed fires only one or two action potentials and then becomes suppressed again. Such short events are not considered as a reversal in our analyses (less than 250 ms), and the dominance durations are determined by neglecting these events (see Supplement Figure S2). Second, there are periods where short events occurred alternatingly between the two neurons with intermingled action potentials from both neurons (Supplement Figure S2). In these periods, none of the two neurons are considered to be dominant. These observations may also be linked to known observations in bi-stable perception. It has been reported that human subjects experience short reversal events detected in reflexes (optokinetic nystagmus and pupil dilations) but they are too short to be reported by the subjects[28]. Furthermore, the intermingled firing of action potentials by the two neurons may be related to the period in bi-stable perception where the perception of the subject is either uncertain or a mixture of the two possible percepts (“composite” or “mixed” perception). The short and the mixture events are potentially important

because they may elucidate the neural mechanisms underlying the stochastic properties of bi-stability and decision-making processes.

Concluding, our experimental model provides a platform for investigating the dynamics of a theoretically derived neural circuit in real-life neurons. Our data showed that even the simplest competition circuit, between two individual pyramidal neurons, already reproduces dynamics of bi-stable perception that we find in human perception.

**Materials and Methods**

Experiments were performed at the Brain Science Institute (Tamagawa University, Japan), and the Donders Institute for Brain, Cognition and Behavior, (Radboud University, The Netherlands). The experimental animal procedures were approved by the Animal Research Ethics Committee of Tamagawa University (animal experiment protocol H29/08) and the Animal Ethics Committee of the Radboud University Nijmegen, under DEC application number 2018-0016 (Nijmegen, the Netherlands). The procedures are in accordance with the Guidelines for Animal Experimentation in Neuroscience (Japan Neuroscience Society) and the Dutch legislation.

**Brain slice preparation**

Brain slices were prepared from the occipital part of the mouse brain that includes the visual cortex (strain C57Bl6/J, age p12 to p24). Mice were anesthetized deeply using isoflurane in an induction chamber. Following deep anesthesia, mice were quickly decapitated and the brain was removed from the skull in a small container with chilled “cutting solution”. For this process, the solution of either one of the following compositions was used (in mM): 125 NaCl, 25 NaHCO3, 2.5 KCl, 1.25 NaH2PO4, 1 $CaCl_2$, 2 $MgCl_2$, 25 D-glucose, or 75 sucrose, 87 NaCl, 25 $NaHCO_3$, 2.5 KCl, 1.25 $NaH_2PO_4$, 0.5 $CaCl_2$, 7 $MgCl_2$, 25 D-glucose, both saturated with 95% $O_2$, 5% $CO_2$. Then, the brain tissue was glued on to the cutting stage of a vibratome (VT1000S, Leica, Germany, or Microm HM 650V, Thermo Scientific, USA), submerged in the cutting solution above. Coronal or angled-

coronal[29] sections of 300~400μm thickness were cut and stored in an incubation chamber in 32~34°C for at least 30 min, and then stored at room temperature until use.

**Double whole-cell recordings**

Slices were transferred to a recording chamber on a microscope stage and were superfused with artificial cerebrospinal fluid, ACSF, maintained at a constant temperature (32~34°C). ACSF had the following composition (in mM): 125 NaCl, 25 $NaHCO_3$, 2.5 KCl, 1.25 $NaH_2PO_4$, 2 $CaCl_2$, 1 $MgCl_2$, 25 D-glucose, saturated with 95% $O_2$, 5% $CO_2$. The location of V1 was identified under the microscope (Olympus, Japan) equipped with DIC-IR (differential interference contrast – infrared). Layers of visual cortex were identified and the point where layer 5 starts thickening, going from medial to lateral, was used as a landmark of the border between V1 and LM (lateromedial area[30], equivalent to V2, Figure 1c). All recordings were made from the region medial from the landmark. Under high magnification with x40 objective, pyramidal neurons in layer 2/3 were identified by their stereotypical morphology. In some cases, the recorded neurons were filled with biocytin and post-experimental process indicated that, in all cases, they were pyramidal neurons in layer 2/3 (see below). Two neurons separated by at least 150μm distance were selected to reduce the probability of choosing connected pairs. Furthermore, experimental protocols were performed to check for monosynaptic (paired-pulse injection at 10Hz to one of the neurons to evoke action potentials) and disynaptic connections[31,32] (100Hz 11 pulses injection to one of the neurons to evoke a train of action potentials). None of the pairs reported in this paper were connected.

Pipettes for patch clamp recordings were pulled from borosilicate thin glass capillaries (TW150-4, WPI, USA) and filled with a filtered intracellular solution with the following composition (mM). 130 K-gluconate, 10 KCl, 4 ATP-Mg, 0.3 Na-GTP, 10 HEPES, 10 phosphocreatine. For phosphocreatine, either 10mM $Na_2$-phosphocreatine or a mixture of 5mM $Na_2$-phosphocreatine and 5mM tris-phosphocreatine was used. The osmolarity of the solution was adjusted to 290~300Osm by either Osmotron-5 (Orion Riken Co., Japan) or Semi-Micro Osmometer K-7400

(Knauer, Germany) and the pH was adjusted to 7.2. The final resistance of the pipettes was 7~9MΩ. In some cases, biocytin was added to the pipette solution (2.5~5mg/ml) to visualize the recorded neurons post-experimentally. Recordings were carried out using either two Axopatch 200B amplifiers or a Multiclamp 700 amplifier (both Molecular Devices, Sunnyvale, CA, USA). Data were lowpass filtered at 10kHz and were digitized at 20 kHz using a Digidata A/D board model 1440A. Data were captured using the Clampex program suite (Molecular Devices, USA). Series resistances were constantly monitored by injecting a −100pA pulse in current-clamp configuration. Series resistances were balanced via a bridge circuit.

**Cell identification**

To visualize the pyramidal neuron pairs that were recorded, they were filled with biocytin by diffusion (N=9). After the recording (approximately 30 to 60 minutes), the slices were kept in 4% paraformaldehyde in phosphate buffer solution, PBS, (0.1 M, pH 7.2) and were kept at 4˚C. After washing the tissue with PBS, it was quenched with 1% $H_2O_2$ in 10% methanol and 90 % PBS for 5 minutes. The tissue was washed with PBS and permeabilized with 2% Triton X-100 in PBS for 1 hour and then put in ABC solution (ABC Elite Kit, Vector, USA) overnight at 4˚C. After washing the tissue with PBS and then with Tris buffer (0.05M), it was processed with DAB solution (0.5g/l in 0.05M Tris buffer) and 1%$H_2O_2$ was added to enhance the reaction. After verifying the visualization of neurons, the tissue was washed by PBS and then mounted to glass slides with a mounting medium (Aquamount, Vector, USA).

**Dynamic clamp**

A modified version of the dynamic clamp system StdpC (spike timing dependent plasticity clamp)[12] was used to establish the connections between recorded neurons and model neurons with model synapses. The communication between the amplifier and StdpC was mediated by a National

Instruments A/D board, model PCIe-6321. Dynamic clamp is a method whereby a modelled conductance, e.g. a synaptic or ionic conductance, is computed based on the measured membrane potential of a neuron, then injected into that neuron in real time with a patch clamp electrode. Unlike other dynamic clamp systems which operate at fixed frequencies, StdpC does not require a real-time operating system, relying instead on precise measurement of the time elapsed in each measure-compute-inject cycle to perform the numerical integration of its models.

Besides numerous improvements to the software interface, the following major additions were made to the previous version of StdpC[12]. A passive membrane model was added, which can be augmented with models of ionic and synaptic conductances to form completely synthetic neuron models. To stabilize numerical integration of such models at StdpC's unpredictable and varying sampling frequency, the clamp cycle was upgraded from explicit Euler to a Runge-Kutta integration scheme of order 4/5. A number of performance enhancements were made to ensure high-frequency, and thus high-fidelity, updates to the injected current. A delay mechanism was added to the synapse models, allowing the simulation of conduction and synaptic delays. Finally, a model of synaptic background noise was added, reproducing the synaptic bombardment we would expect to see in vivo with statistically equivalent, randomly generated inhibitory and excitatory currents, as described in the section on noise below. The upgraded version of StdpC (StdpC version 6.1) is available at github.com (github.com/CompEphys-team/stdpc, DOI 10.5281/zenodo.3492203).

A custom-made summing circuit was used to combine the command signal from StdpC and the one from Clampex software, and the combined command signal was fed to the amplifier.

Hodgkin-Huxley models of ionic channels (conventional sodium, delayed rectifier potassium, and Kv3 potassium channels) were given to the model inhibitory neuron (membrane capacitance 0.2115nF, leak conductance 63.462nS, equilibrium potential for the leak conductance -70mV[33]). A Kv3 channel was added to simulate fast spiking inhibitory neurons[34]. The models are based on an "$\alpha/\beta$ formalism" as follows (see github.com/CompEphys-team/stdpc/tree/master/manual).

$$I = g_{max} m^p h^q (V - V_{rev})$$

$$\frac{dm}{dt} = \alpha_m (1 - m) - \beta_m m$$

$$\alpha_m = k_{\alpha,m} F_{\alpha,m} \left( \frac{V - V_{\alpha,m}}{s_{\alpha,m}} \right)$$

$$\beta_m = k_{\beta,m} F_{\beta,m} \left( \frac{V - V_{\beta,m}}{s_{\beta,m}} \right)$$

(and analogous for *h*).

Here, *m* and *h* are activation and inactivation variables. $g_{max}$ is the maximum conductance of the ion channel and $V_{rev}$ is the reversal potential of the ion. The form of the function *F* is either one of the three below.

$$F_1(x) = \frac{x}{\exp(x) - 1}$$

$$F_2(x) = \exp\,(x)$$

$$F_3(x) = \frac{1}{1 + \exp\,(x)}$$

For the potassium channels, the formalisms are the same, except that no inactivation components are included. The form of the function *F* and the parameters for $\alpha$ and $\beta$ for the individual components are as summarized in Table S1 (top). These parameter values were taken from Pospischil *et al.*[33] for basic membrane properties, from Hodgkin & Huxley[35] for sodium and delayed rectifier potassium channels and from Lien & Jonas[34] for KV3 channel.

Conductance of excitatory and inhibitory synaptic events were modeled using the ChemSyn model in StdpC, following the equations and parameters described below.

$$I = g_{syn}S(t)(V_{syn} - V_{post}(t))$$

$$\tau_{syn}\frac{dS(t)}{dt} = \frac{S_\infty\big(V_{pre}(t)\big) - S(t)}{1 - S_\infty\big(V_{pre}(t)\big)}$$

$$S_\infty\big(V_{pre}(t)\big) = \begin{cases} \tanh\left(\dfrac{V_{pre}(t) - V_{TH}}{V_{slope}}\right) & if\ V_{pre}(t) > V_{TH} \\ 0 & otherwise \end{cases}$$

Parameters for excitatory and inhibitory synapses are shown in Table S1 (middle). *G_syn* for EPSP was selected so that it evokes an action potential in mINs (Fig. S1), and *g_syn* and *τ_syn* for IPSP were selected to ensure strong enough suppression of target PN. The synaptic delay was set to 1ms in all cases, and no synaptic plasticity was included in the model.

**Disynaptic mutual inhibition connections**

Establishment of a mutual inhibition circuit was verified as follows. Injection of a brief (1ms) depolarization current (1500~2000pA) to one of the pairs of pyramidal neurons evoked an action potential (red and blue triangles in Fig. S1a), which triggered an excitatory synaptic conductance in the model inhibitory neuron. This synaptic event evoked an EPSP in the inhibitory neuron. As shown in Fig. S1a, when $g_{Max}$ was set to 10nS or higher, the EPSP evoked an action potential (red and blue disks). This action potential in the inhibitory neuron triggered an inhibitory synaptic conductance, which was fed to the postsynaptic pyramidal neuron as an injected IPSC via the amplifier, giving rise to a corresponding IPSP (blue and red asterisks). Fig. S1a shows that an action potential was first evoked in the pyramidal neuron 1 (PN1) and the pyramidal neuron 2 (PN2) received an IPSP. Later, an action potential was evoked in PN2 that resulted in an IPSP given to PN1, illustrating that the mutual inhibition circuit was established between the two pyramidal neurons by this system. As shown in Fig. S1b, the inhibitory neurons show trains of action potentials corresponding to the action potentials of presynaptic pyramidal neurons during bi-stable activity.

**Bi-stable activity**

Bi-stable activity is evoked by the following protocol. First, before the dynamic clamp mediated model circuit is switched on, depolarization currents that evoke action potentials at approximately 10 Hz in the two neurons are determined separately. Next, the model circuit is switched on to activate the mutual inhibitory connection, and the depolarization currents as determined above are injected. In most cases, this already produces bi-stable activity in the pair (unless one of the neurons is 100% dominant). However, every neuron has different firing patterns, different degrees of responses to given synaptic inputs, and different sizes of action potentials (which influence the strength of postsynaptic events). As a result, the bi-stable activity often does not show equal dominance between the two neurons even though the firing rates are equivalent between them. Therefore, in the case that it is necessary to find the current pair where the dominance of the two neurons are approximately equal (50% dominance point), the currents are further adjusted by either increasing the current in the weaker neuron or decreasing the current in the stronger neuron.

Dominance, dominance durations, and reversal rates were calculated using custom Matlab (MathWorks, USA) scripts. Unlike behavioral studies, in which a dominant percept is indicated as a continuous signal (by button press), the dominance of a neuron is signaled by sustained repetitive firing of action potentials. Hence, we defined the “dominance duration” of a neuron as follows (illustrated in Fig. S2). First, a continuous firing of action potentials in one neuron until an action potential occurs in the other neuron is considered as a tentative dominance duration of the neuron (Fig. S2b). Hence, at this stage, the dominance durations of the two neurons are mutually exclusive. Note that there are short dominance durations (blue asterisks for PN2 and red asterisk for PN1). There are also a series of alternations of short dominance durations between the two neurons (green asterisks). Next, dominance durations shorter than 250ms are eliminated (Fig. S2c). This process results in short lags between the dominance durations (blue and red asterisks). The occurrence of the short lag is not considered as reversal and, hence, the previous dominance is

considered to continue (arrows). These processes result in the final dominance durations without short durations (Fig. S2d). Note that there are also the intervals that are not assigned to either of the neurons corresponding to the period marked with green asterisks in Fig. S2c. This is because alternating short durations occur between the two neurons during these periods (Fig. S2c green asterisks). These periods are assigned as “both active” (Fig. S2d bottom). Dominance and reversal rates were computed based on this definition of dominance durations. “Dominance” of a neuron is defined as the ratio of total dominance durations of the neuron (sum of all dominance durations of the neuron) divided by the sum of the total dominance durations of both neurons. A reversal is defined as the dominance switching from one neuron to the other, regardless of the presence or absence of a “both active” phase during the switch.

Special attention was paid to the recording conditions. If the following criterion were not met, the recording was halted: The overshoot of action potential should be higher than 10mV, and changes in the size of the action potential, in series resistance, and in firing rate to a given depolarization current should be less than 15% during data collection.

**Analysis of adaptation**

Inter-spike intervals and the peaks of action potentials were estimated with custom Matlab scripts. Upon detection of action potentials inter-spike intervals and the peaks were measured. These values were plotted against time to visualize the progress of adaptation within individual dominance episodes (Figure 3a, b). To pool the data, first, the time from the onset of the dominance cycle to the end of this cycle was normalized by dividing it by the cycle’s dominance duration (for the individual cycles of the individual pairs), resulting in the normalized time ranging from 0 to 1. Second, inter-spike intervals and the magnitude of action potential peaks were normalized by the first values of the individual cycles. Third, the normalized values across all pairs were sorted into bins of size 0.01. Finally, the mean and standard deviation of all inter-spike intervals and action potential peaks in a given bin were plotted against the normalized time (Figure 3c and 3d). As an

indicator of the progress of adaptation, inter-spike intervals (normalized by the mean of individual pair) was plotted over time from the onset of each dominance cycle and linear regression was applied to the plot (Fig. S3). This resulted in slope values that indicated the change of inter-spike intervals. To pool the data, the dominance durations of individual pairs were normalized by their mean values and the slopes, normalized by the mean values of individual neurons, were plotted over the normalized duration (Figure 3f).

**Effect of noise**

To investigate the effect of noise on the dynamics of bi-stable activity, synaptic background activity was simulated according to the model by Destexhe et al.[18]. In their simulation, random walk-like fluctuations of membrane conductance were modeled by applying the Ornstein-Uhlenbeck model of Brownian motion[36]. Their formalism of synaptic noise was implemented in the StdpC dynamic clamp system. The evolution of the simulated synaptic noise depends on the noise time constant $\tau$, which controls noise color, as well as the mean $g_{mean}$ and standard deviation $SD_g$ of the noise, and is modeled as follows:

$$I = g(t)(V_{rev} - V)$$

$$g(t + \Delta t) = g_{mean} + (g(t) - g_{mean})\, e^{-\frac{\Delta t}{\tau}} + Ar$$

$$A = \sqrt{\frac{D\tau}{2}\left(1 - e^{-\frac{2\Delta t}{\tau}}\right)}$$

Here, $r$ is a pseudo-random number drawn from a normal distribution with mean 0 and standard deviation 1, and the noise diffusion coefficient $D$ is related to the noise standard deviation as follows:

$$D = \frac{2\, SD^2{}_g}{\tau}$$

Excitatory and inhibitory synaptic noise are modeled separately. The level of noise is expressed as the standard deviation $SD_g$ of the synaptic conductance and systematically manipulated, whereas the average conductance $g_{mean}$, which functions as a constant current offset, remained unchanged. The amount of noise given to mINs was larger than that given to PNs because PNs already have intrinsic synaptic noise (Figure 4a) from their presynaptic neurons within the brain slice. The standard parameter set (used as default unless mentioned otherwise) for the noise is shown in Table S1 (bottom).

In the experiments for the effect of noise level and the effect of activation level (below), the length of each trial was 200 sec with 193.5 sec long depolarization current.

**Paradigms equivalent to Levelt's experiments**

For our experiments associated with the classic behavioral experiments of Levelt[20], we systematically varied the strength of the sustained depolarization current into one, or both, of the pyramidal neurons. Concerning Levelt's proposition I to III, only one of the two currents (randomly selected) was altered. The change of the current was made by steps of 10 or 20pA.

In the analyses, the current that would evoke 50% dominance, called $I_{50\%}$, was estimated by linear regression of dominance over the changing current. The change of the current is reported with reference to this control current value, defined as follows.

$$\Delta I_{50\% norm} = \frac{I - I_{50\%}}{I_{50\%}}$$

Hence, in the plots in Figure 5c to 5h, the right side from x=0 indicates that the neuron that received the changing current was more dominant (stronger) than the other neuron and the left side indicates the former being weaker than the latter. Before pooling the data (N=46) for average durations, average dominance durations of individual trials were computed and were divided by the maximum

average duration within individual neuron. To pool the data for the reversal rate, data were normalized by the maximum reversal rate of the individual pair (Fig 5h).

Concerning Levelt's proposition IV, both currents were modified. First, a current pair that evoked a 10Hz firing rate in the two neurons was found. If necessary, the current was adjusted until the current pair evoked approximately 50% dominance. This current pair was considered as a control and is called $I_{10Hz}$ (it is called as such for convenience although the current pair did not always evoke 10Hz firing). Next, in one of the two neurons, the current was changed with 10 or 20pA steps and the current for the other neuron was changed proportionally. To pool the data, the change of the current is reported with reference to $I_{10Hz}$, defined as follows.

$$\Delta I_{10Hznorm} = \frac{I - I_{10Hz}}{I_{10Hz}}$$

To pool the data for the reversal rate (N=32), data were normalized by the reversal rate of the individual pair when the control current pair was used (Fig 6c).

To make the bar plots of the pooled data (Figure 5f to h, right, Figure 6c bottom), the $\Delta I$ was binned and the values in the individual bins were averaged. The order of trials with different current pairs was pseudo-randomly chosen.

For statistical analysis, repeated measures analysis of variance (ANOVA) was applied using SPSS Statistics (IBM, USA). Pairs with the standard noise parameter set for the experiment of noise (N=15), pairs with injected current of $I_{50\%}$ in Levelt I to III paradigms (N=46), and pairs with injected current of $I_{10Hz}$ in Levelt IV paradigm (N=32) are collectively called a "control pair" and statistical analyses were performed on these 93 pairs to report basic properties of bi-stability and adaptation. Error bars in the plots are +/- SEM.

All data and Matlab codes for data analyses are published at Radboud University data repository site with URL as below.

https://data.donders.ru.nl/collections/di/dcn/DAC_626810_0008_424?93

**Acknowledgments**

We would like to thank Dr. Ginamaria Maccaferri (Northwestern University, Chicago, USA) for supporting the project during the time of piloting, Dr. Andreas Burkhalter (Washington University, St. Louis, USA) for providing detailed information of the anatomy of mouse visual cortex, Dr. Yoshikazu Isomura (Tamagawa University, Machida, Japan) for supporting to conduct the project and the anatomical analysis at Brain Science Institute, Dr. Nael Nadif Kasri and Dr. Dirk Schubert (RadboudUMC, Nijmegen, The Netherlands) for supporting to run the experiments at their laboratory. Naoki Kogo was supported by a post-doctoral fellowship of Fonds voor Wetenschappelijk Onderzoek (FWO-Flanders post-doc grant 12L5115N, University of Leuven, 2014~2017) and a European Fellowship from Marie Curie Actions (794273, Radboud University, 2018~current). TN was supported by the EPSRC (EP/P006094/1) and European Union (785907).

**References**

1. Leopold & Logothetis. Multistable phenomena: changing views in perception. *Trends Cogn. Sci. (Regul. Ed.)* **3**, 254–264 (1999).
2. Bonds, A. B. Role of inhibition in the specification of orientation selectivity of cells in the cat striate cortex. *Vis. Neurosci.* **2**, 41–55 (1989).
3. Sillito, A. M. The contribution of inhibitory mechanisms to the receptive field properties of neurones in the striate cortex of the cat. *J Physiol* **250**, 305–329 (1975).
4. Mikami, A., Newsome, W. T. & Wurtz, R. H. Motion selectivity in macaque visual cortex. I. Mechanisms of direction and speed selectivity in extrastriate area MT. *J. Neurophysiol.* **55**, 1308–1327 (1986).
5. Snowden, R. J., Treue, S., Erickson, R. G. & Andersen, R. A. The response of area MT and V1 neurons to transparent motion. *J. Neurosci.* **11**, 2768–2785 (1991).

6. Zhou, H., Friedman, H. S. & von der Heydt, R. Coding of border ownership in monkey visual cortex. *Journal of Neuroscience* **20**, 6594–6611 (2000).
7. Kogo, N. & van Ee, R. Neural mechanisms of figure-ground organization: Border-ownership, competition and perceptual switching. in *Oxford Handbook of Perceptual Organization* 342–362 (Oxford University Press, 2015).
8. Masquelier, T., Guyonneau, R. & Thorpe, S. J. Competitive STDP-based spike pattern learning. *Neural Comput* **21**, 1259–1276 (2009).
9. Machens, C. K., Romo, R. & Brody, C. D. Flexible control of mutual inhibition: a neural model of two-interval discrimination. *Science* **307**, 1121–1124 (2005).
10. Usher, M. & McClelland, J. L. The time course of perceptual choice: the leaky, competing accumulator model. *Psychol Rev* **108**, 550–592 (2001).
11. Mark, S., Romani, S., Jezek, K. & Tsodyks, M. Theta-paced flickering between place-cell maps in the hippocampus: A model based on short-term synaptic plasticity. *Hippocampus* **27**, 959–970 (2017).
12. Nowotny, T., Szucs, A., Pinto, R. D. & Selverston, A. I. StdpC: a modern dynamic clamp. *J. Neurosci. Methods* **158**, 287–299 (2006).
13. Kemenes, I. *et al.* Dynamic clamp with StdpC software. *Nat Protoc* **6**, 405–417 (2011).
14. Brascamp, J. W., van Ee, R., Noest, A. J., Jacobs, R. H. & van den Berg, A. V. The time course of binocular rivalry reveals a fundamental role of noise. *Journal of Vision* **6**, 1244–56 (2006).
15. Moreno-Bote, R., Rinzel, J. & Rubin, N. Noise-induced alternations in an attractor network model of perceptual bistability. *J. Neurophysiol.* **98**, 1125–1139 (2007).
16. Kim, Y.-J., Grabowecky, M. & Suzuki, S. Stochastic resonance in binocular rivalry. *Vision Res.* **46**, 392–406 (2006).
17. Shpiro, A., Moreno-Bote, R., Rubin, N. & Rinzel, J. Balance between noise and adaptation in competition models of perceptual bistability. *J Comput Neurosci* **27**, 37–54 (2009).

18. Destexhe, A., Rudolph, M., Fellous, J.-M. & Sejnowski, T. J. Fluctuating synaptic conductances recreate in vivo-like activity in neocortical neurons. *Neuroscience* **107**, 13–24 (2001).
19. Delgado, J. Y., Gómez-González, J. F. & Desai, N. S. Pyramidal neuron conductance state gates spike-timing-dependent plasticity. *J. Neurosci.* **30**, 15713–15725 (2010).
20. Levelt, W. J. M. *On binocular rivalry*. (Institute for Perception RVO-TNO, 1965).
21. Matsuoka, K. The dynamic model of binocular rivalry. *Biol. Cybern.* **49**, 201–208 (1984).
22. Noest, A. J., van Ee, R., Nijs, M. M. & van Wezel, R. J. Percept-choice sequences driven by interrupted ambiguous stimuli: a low-level neural model. *Journal of Vision* **7**, 10 1-14 (2007).
23. Lankheet, M. J. M. Unraveling adaptation and mutual inhibition in perceptual rivalry. *J Vis* **6**, 304–310 (2006).
24. Wilson, H. R., Krupa, B. & Wilkinson, F. Dynamics of perceptual oscillations in form vision. *Nat. Neurosci.* **3**, 170–176 (2000).
25. Alais, D., Cass, J., O'Shea, R. P. & Blake, R. Visual sensitivity underlying changes in visual consciousness. *Current Biology* **20**, 1362–1367 (2010).
26. Levelt, W. J. Note on the distribution of dominance times in binocular rivalry. *Br J Psychol* **58**, 143–145 (1967).
27. Brascamp, J. W., Klink, P. C. & Levelt, W. J. M. The 'laws' of binocular rivalry: 50 years of Levelt's propositions. *Vision Res.* **109**, 20–37 (2015).
28. Naber, M., Frässle, S. & Einhäuser, W. Perceptual Rivalry: Reflexes Reveal the Gradual Nature of Visual Awareness. *PLoS ONE* **6**, e20910 (2011).
29. Dong, H., Shao, Z., Nerbonne, J. M. & Burkhalter, A. Differential depression of inhibitory synaptic responses in feedforward and feedback circuits between different areas of mouse visual cortex. *J. Comp. Neurol.* **475**, 361–373 (2004).
30. Wang, Q. & Burkhalter, A. Area map of mouse visual cortex. *Journal of Comparative Neurology* **502**, 339–357 (2007).

31. Silberberg, G. & Markram, H. Disynaptic inhibition between neocortical pyramidal cells mediated by Martinotti cells. *Neuron* **53**, 735–746 (2007).

32. Kapfer, C., Glickfeld, L. L., Atallah, B. V. & Scanziani, M. Supralinear increase of recurrent inhibition during sparse activity in the somatosensory cortex. *Nat. Neurosci.* **10**, 743–753 (2007).

33. Pospischil, M. *et al.* Minimal Hodgkin-Huxley type models for different classes of cortical and thalamic neurons. *Biol Cybern* **99**, 427–441 (2008).

34. Lien, C.-C. & Jonas, P. Kv3 potassium conductance is necessary and kinetically optimized for high-frequency action potential generation in hippocampal interneurons. *J. Neurosci.* **23**, 2058–2068 (2003).

35. Hodgkin, A. L. & Huxley, A. F. A quantitative description of membrane current and its application to conduction and excitation in nerve. *J Physiol* **117**, 500–544 (1952).

36. Uhlenbeck, G. E. & Ornstein, L. S. On the Theory of the Brownian Motion. *Phys. Rev.* **36**, 823–841 (1930).

**Figures captions**

**Figure 1.** Mutual inhibition circuit and experimental design. **a**: Neural circuit diagram for a mutual inhibition circuit. Triangles: pyramidal neurons (PNs). Disks: inhibitory neurons (INs). **b**: The bi-directional disynaptic mutual inhibition circuit was established between two real-life pyramidal neurons by implementing model inhibitory neurons and synapses (dashed lines) in the StdpC dynamic clamp system. **c**: An image of the brain slice (right hemisphere) from a DIC-IR (differential interference contrast – infrared) microscope during recording with two patch recording pipettes placed in layer 2/3 of V1. 1 to 6: six layers in V1. LM: lateromedial area (equivalent to V2). d: dorsal, v: ventral, l: lateral, m: medial. Scale bar: 200 μm. **d**: An example of biocytin filled pair of pyramidal neurons. Scale bar: 50 μm.

**Figure 2.** Mutual inhibition between a pair of pyramidal neurons and bi-stable activity. **a**: With the dynamic clamp mediated mutual inhibition circuit established, an action potential (red triangle) in the first pyramidal neuron (PN1) triggers an inhibitory postsynaptic potential (IPSP, blue asterisk) in the second pyramidal neuron (PN2); similarly, an action potential of PN2 (blue triangle) causes an IPSP in PN1 (red asterisk). Traces are an average of 5 trials. Baseline membrane potentials were set to -60mV in both neurons. **b**: Continuous injection of depolarization currents into the two pyramidal neurons produces bi-stable activity with alternating dominance between them. MP: membrane potential (mV). MC: membrane current (pA). Inset: The response of the same pyramidal neurons to the same depolarization current injection without the mutual inhibition circuit, showing

sustained continuous firing of action potentials. **c**: The part of data (orange rectangle) shown in B. Upon the onset of the current injection, while both neurons started to depolarize, PN2 was the first to fire an action potential. As a result, PN1 received an IPSP causing PN2 to become dominant and PN1 suppressed. **d**: The part of data around the time of reversal. The inter-spike interval increased during the dominant period of PN2 due to adaptation. Just after the rightmost action potential of PN2, PN1 got a sufficient period of time to recover from its IPSP, enabling it to reach its firing threshold before PN2 was able to fire its next action potential. The action potential of PN1 now resulted in an IPSP in PN2 entailing a reversal of dominance.

**Figure 3** Adaptation of dominant neuron and its correlation to dominance duration. **a-b**: The physiological signatures of adaptation. Inter-spike intervals (**a**) and the peaks of action potentials (**b**) change due to adaptation during dominance episodes (inter-spike intervals increase and the size of action potentials decreases). **c-d**: Average of inter-spike intervals (**c**) and the action potential peaks (**d**) for pooled data of all 93 "control pairs" (see Methods for the definition). **e**: Slope of inter-spike interval as a function of dominance durations, showing the inverse correlation between them. To compute the slope, linear regression was applied to inter-spike intervals as a function of time from the onset of dominance episode. **f**: Inverse correlation between the slope of inter-spike interval and dominance duration in the pooled data. The dominance durations of individual pairs were normalized by their mean values before pooling. The normalized duration was binned and the pooled data was averaged for the individual bins. Error bars indicate +/- SEM.

**Figure 4** Effect of noise. Model excitatory and inhibitory synaptic noise (random changes of excitatory and inhibitory conductance, gE and gI, respectively) was applied to the pyramidal neurons and the inhibitory neurons through the dynamic clamp system. **a-b**: Baseline membrane potentials at -60mV without (**a**) and with (**b**) the model noise. **c**: Effect of changing the noise level systematically. Increase of the noise resulted in increase of reversal rate (from top to bottom). Noise levels are indicated as standard deviations (SD) of gE and gI (in nS). Asterisk: Data with the "standard" noise parameter set. **d**: Pooled data of the effect of noise to the reversal rates (N=15). The reversal rates from the individual pair are normalized by the value at the standard noise parameters (iii) before pooling. Orange bar (i) indicates the data with no model noise. Error bars indicate +/- SEM. The noise parameter sets for i (no model noise), ii, iii (standard noise parameters), iv and v are shown in the table below. The noise level is increased linearly from ii to v. **e**: Histogram of dominance durations for PN1 and PN2 from 10 minutes continuous recording (with the "standard" noise parameters).

**Figure 5** Results of paradigm equivalent to Levelt's paradigm for proposition I to III. **a**: Schematics of the paradigm equivalent to Levelt's experimental paradigm for bi-stable perception. The level of injected current to either one or both of the two mutually inhibiting pyramidal neurons was systematically changed (analogous to the change of the contrasts in Levelt's experiments). **b**: Example data of the experiment equivalent to Levelt's experimental paradigm for proposition I to III. The level of depolarization current in PN1 was increased (from top to bottom) while the current to PN2 was kept constant. **c-e**: Changes in dominance (**c**), dominance duration (**d**), and reversal rate (**e**) for this pair. PN1 red, PN2 blue. **f-h**: Pooled data (N=46) plotted over the normalized injected current (see Methods). The dominance durations are normalized for the maximum values of the individual neurons. Red: responses of the neurons that received the changes of the injected current. Blue: responses of the neurons whose injected current was kept constant. Left column: The data of the individual pairs. Right column: The normalized current was binned and the pooled data were averaged for the individual bins. Error bars indicate +/- SEM.

**Figure 6** Results of paradigm equivalent to Levelt's paradigm for proposition IV. **a**: The effect of increasing the depolarization currents simultaneously in both pyramidal neurons (from top to bottom). **b**: The changes of the reversal rate for this pair. **c**: Pooled data of reversal rate (N=32) plotted over the normalized injected current (see Methods).

Fig. 1

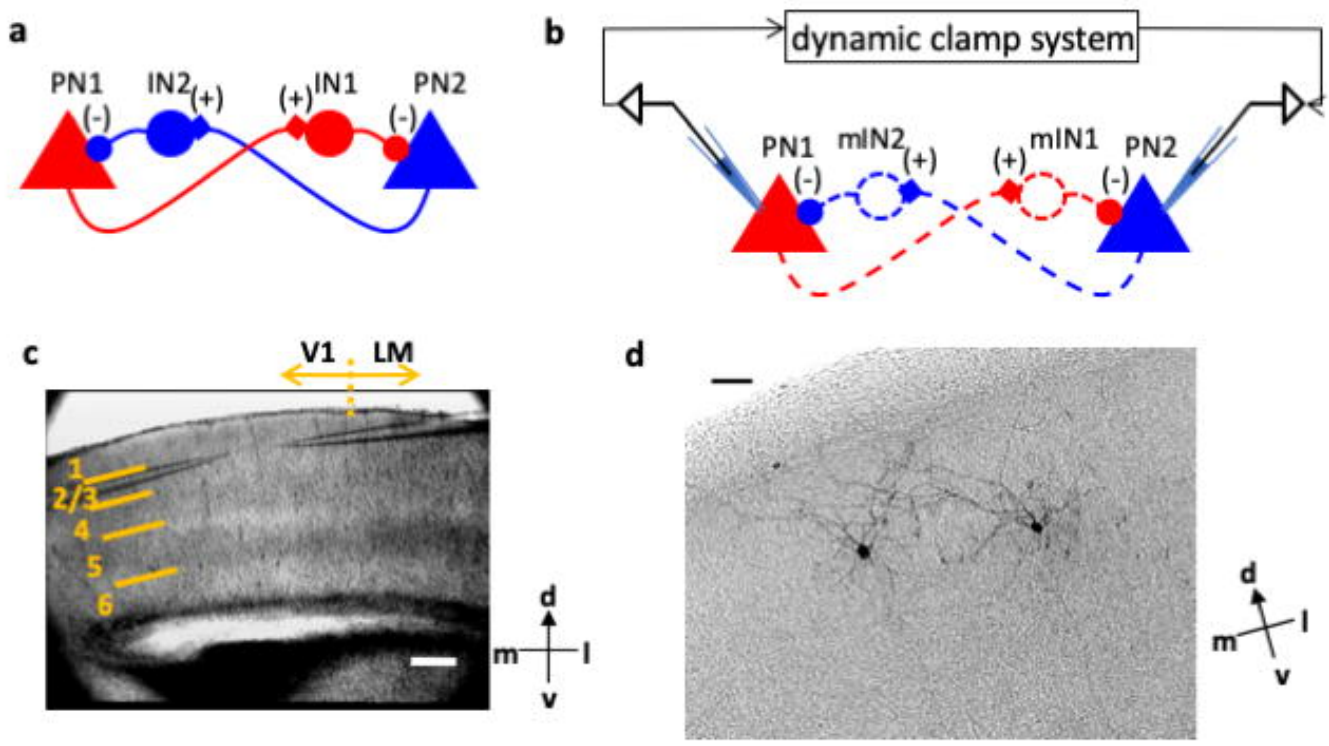
a
PN1
IN2
(+)
(-)
(+)
IN1
(-)
PN2
b
dynamic clamp system
PN1
mIN2
(+)
(-)
(+)
mIN1
(-)
PN2
c
V1
LM
1
2/3
4
5
6
d
m
l
v
d
m
l
v

Fig. 2

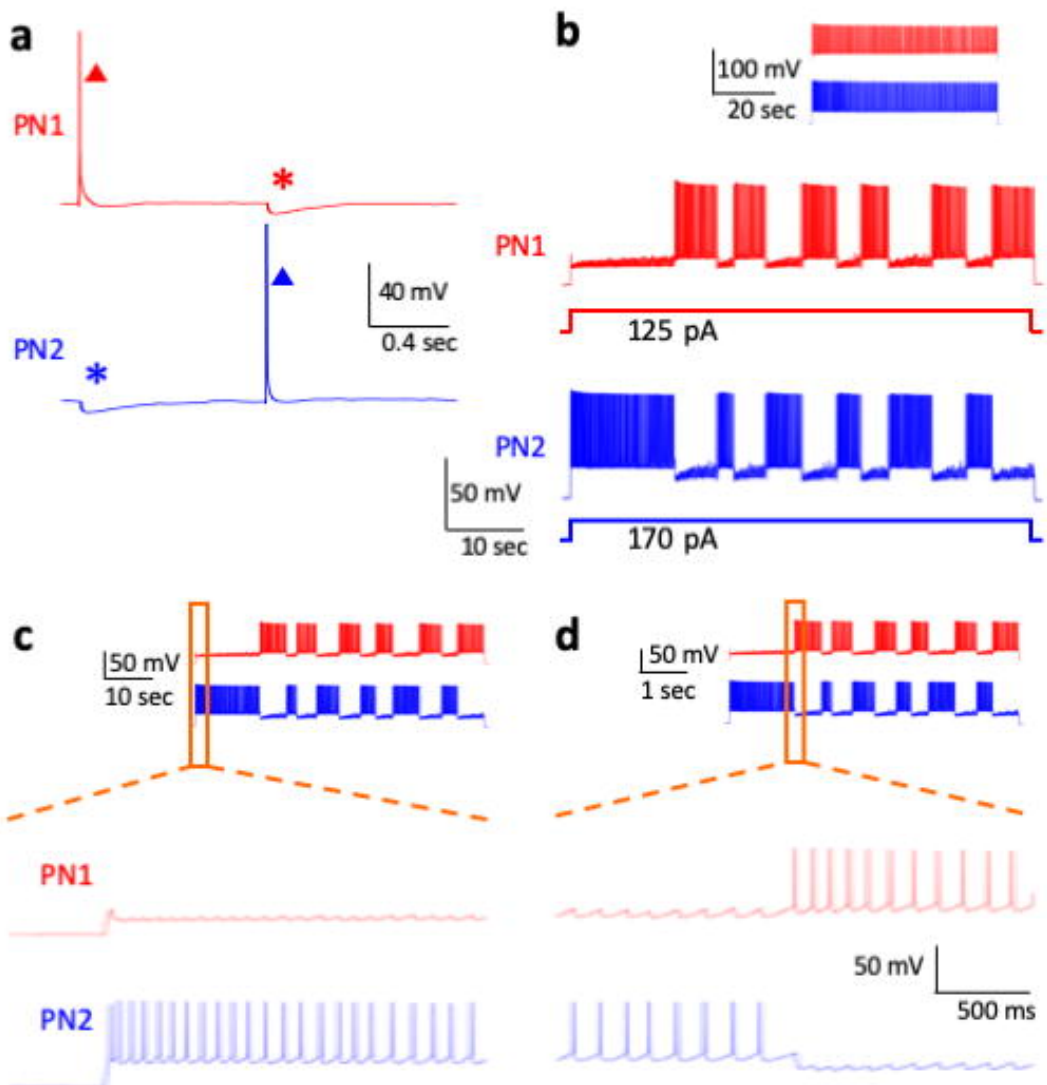
a
PN1
PN2
40 mV
0.4 sec
b
100 mV
20 sec
PN1
125 pA
PN2
50 mV
10 sec
170 pA
c
50 mV
10 sec
PN1
PN2
d
50 mV
1 sec
50 mV
500 ms

Fig. 3

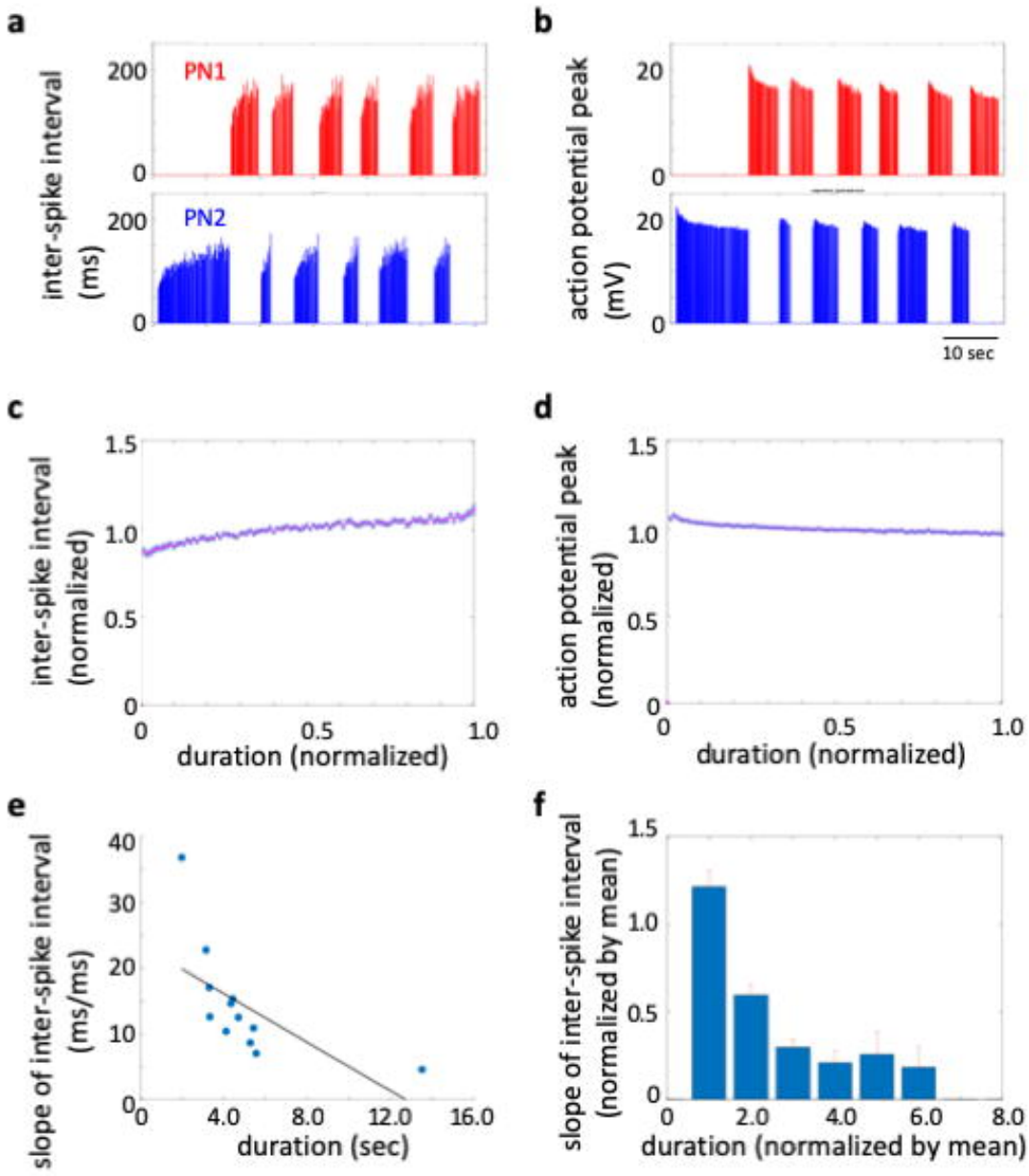
a
inter-spike interval (ms)
200
0
PN1
200
0
PN2
b
action potential peak (mV)
20
0
20
0
10 sec
c
inter-spike interval (normalized)
1.5
1.0
0.5
0
0
0.5
1.0
duration (normalized)
d
action potential peak (normalized)
1.5
1.0
0.5
0
0
0.5
1.0
duration (normalized)
e
slope of inter-spike interval (ms/ms)
40
30
20
10
0
0
4.0
8.0
12.0
16.0
duration (sec)
f
slope of inter-spike interval (normalized by mean)
1.5
1.0
0.5
0
0
2.0
4.0
6.0
8.0
duration (normalized by mean)

Fig. 4

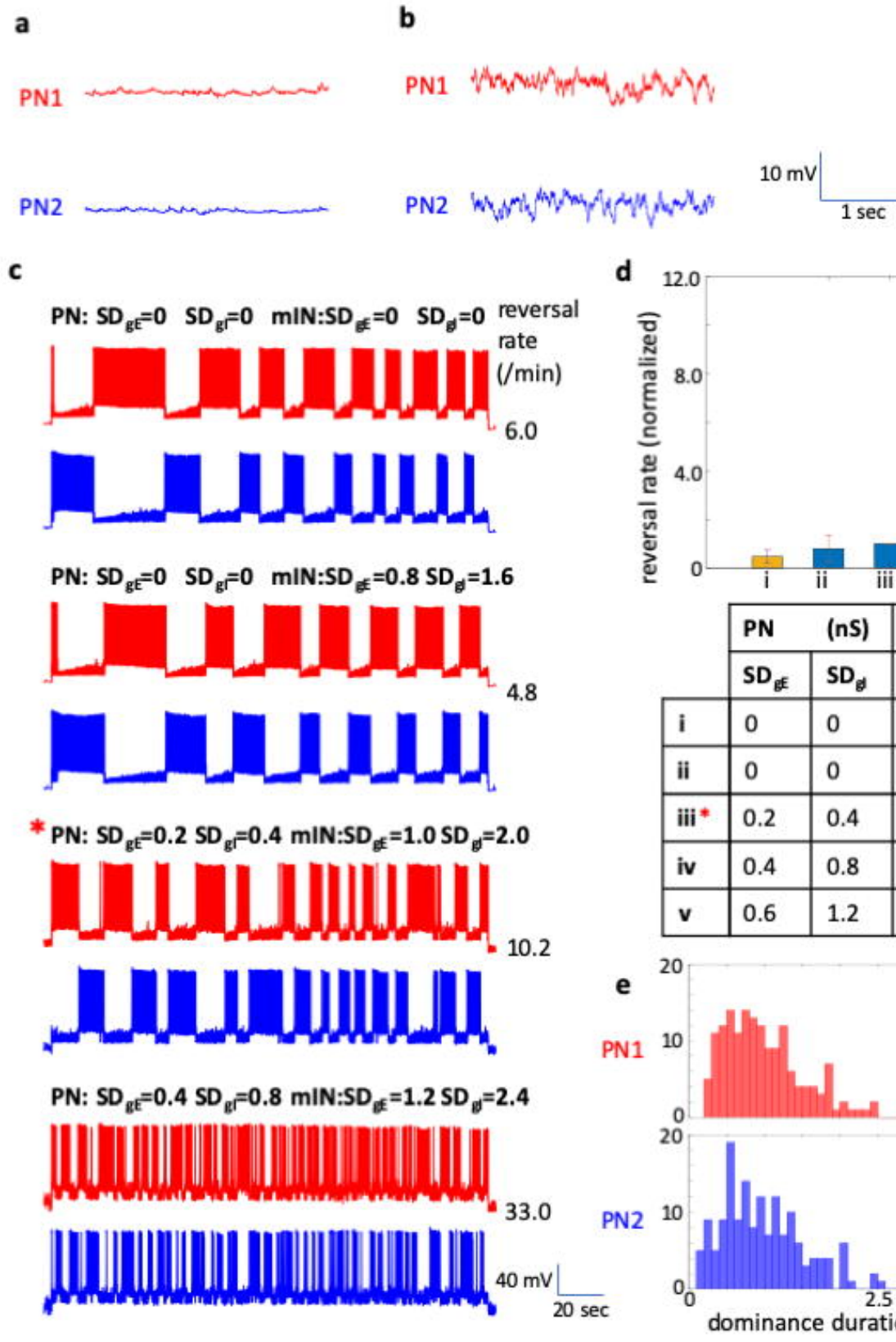


| | PN | (nS) | mIN | (nS) |
|---|---|---|---|---|
| | $SD_{gE}$ | $SD_{gI}$ | $SD_{gE}$ | $SD_{gI}$ |
| i | 0 | 0 | 0 | 0 |
| ii | 0 | 0 | 0.8 | 1.6 |
| iii * | 0.2 | 0.4 | 1.0 | 2.0 |
| iv | 0.4 | 0.8 | 1.2 | 2.4 |
| v | 0.6 | 1.2 | 1.4 | 2.8 |

Fig. 5

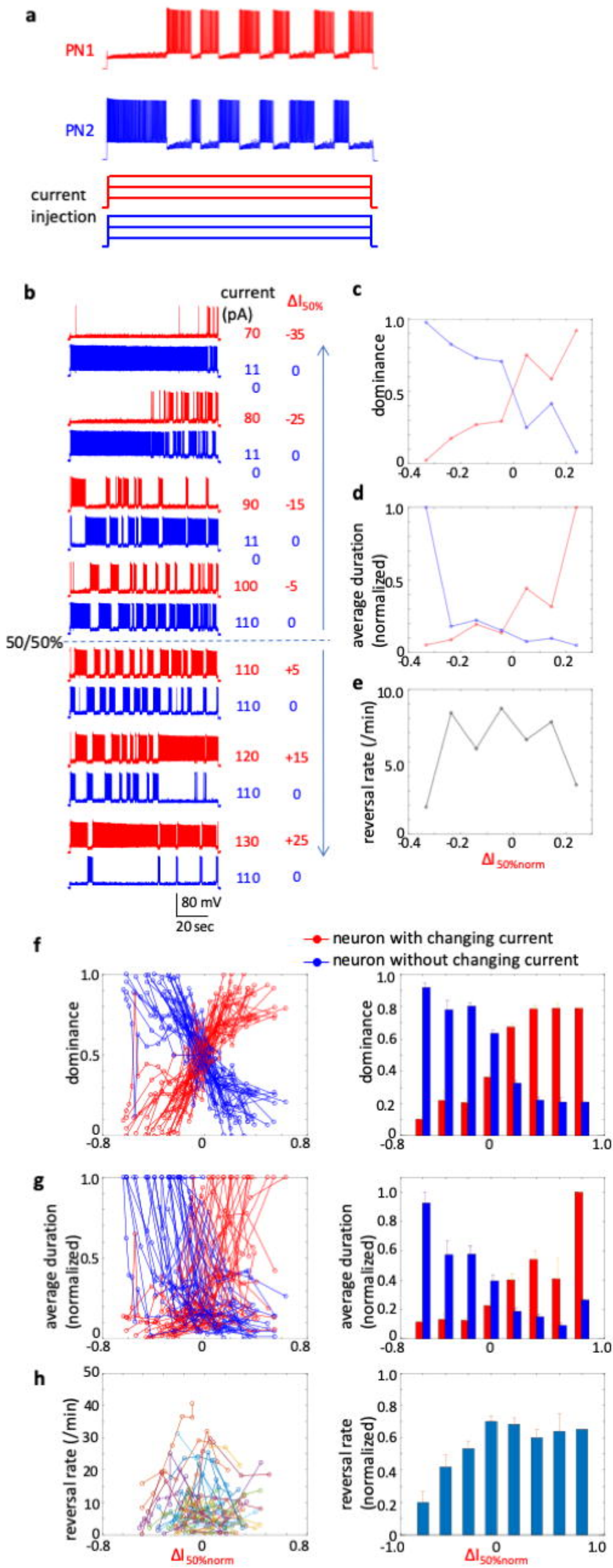
a
PN1
PN2
current injection
b
current (pA)
ΔI50%
70 -35
11 0
0
80 -25
11 0
0
90 -15
11 0
0
100 -5
110 0
50/50%
110 +5
110 0
120 +15
110 0
130 +25
110 0
80 mV
20 sec
c
dominance
d
average duration (normalized)
e
reversal rate (/min)
ΔI50%norm
f
neuron with changing current
neuron without changing current
dominance
g
average duration (normalized)
h
reversal rate (/min)
reversal rate (normalized)
ΔI50%norm

Fig. 6

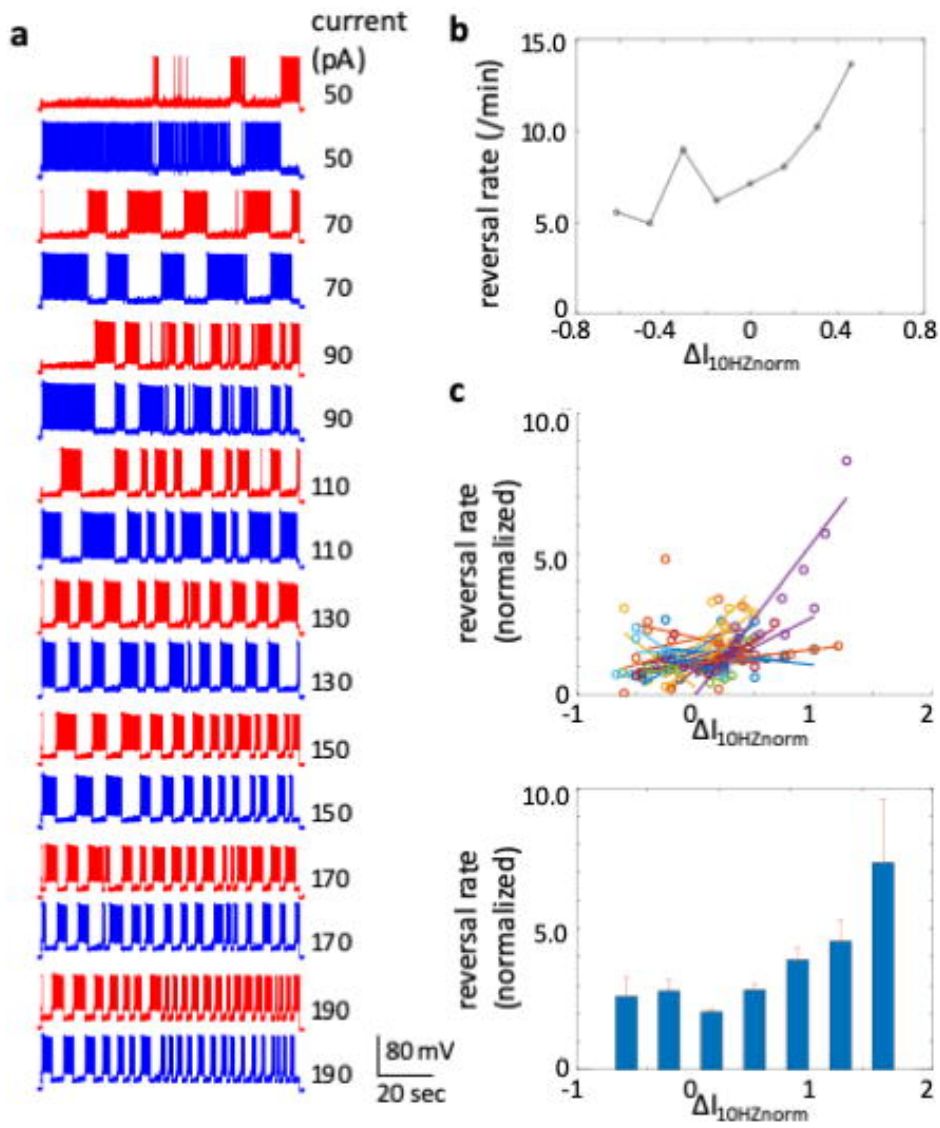
a
current (pA)
50
50
70
70
90
90
110
110
130
130
150
150
170
170
190
190
80 mV
20 sec
b
reversal rate (/min)
15.0
10.0
5.0
0
-0.8
-0.4
0
0.4
0.8
ΔI10HZnorm
c
reversal rate (normalized)
10.0
5.0
0
-1
0
1
2
ΔI10HZnorm
reversal rate (normalized)
10.0
5.0
0
-1
0
1
2
ΔI10HZnorm